G9a/GLP inhibition during ex vivo lymphocyte expansion increases in vivo cytotoxicity of engineered TCR-T cells against hepatocellular carcinoma

Maxine Lam
Institute of Molecular and Cell Biology, Agency for Science, Technology and Research (A*STAR)
Jose Reales-Calderon
Institute of Molecular and Cell Biology, Agency for Science, Technology and Research (A*STAR)
Jin Rong Ow
Institute of Molecular and Cell Biology, Agency for Science, Technology and Research (A*STAR)
Joey AW
Institute of Molecular and Cell Biology, Agency for Science, Technology and Research (A*STAR)
Damien TAN
Institute of Molecular and Cell Biology, Agency for Science, Technology and Research (A*STAR)
Erica Ceccarello
Institute of Molecular and Cell Biology, Agency for Science, Technology and Research (A*STAR)
TOMMASO TABAGLIO
Institute of Molecular and Cell Biology, Agency for Science, Technology and Research (A*STAR)
Yan Ting Lim
Institute of Molecular and Cell Biology
Loo Chien Wang
Agency for Science, Technology and Research
Radoslaw Sobota
Institute of Molecular and Cell Biology, Agency for Science, Technology and Research (A*STAR)
https://orcid.org/0000-0002-2455-2526
Giulia Adriani
Singapore Immunology Network (SIgN), Agency for Science, Technology and Research (A*STAR)
https://orcid.org/0000-0002-7505-1668
Antonio Bertoletti
DUKE-NUS Medical School https://orcid.org/0000-0002-2942-0485
Ernesto Guccione
Tisch Cancer Institute
Andrea PAVESI (andreap@imcb.a-star.edu.sg)
Institute of Molecular and Cell Biology, Agency for Science, Technology and Research (A*STAR)

Article

Keywords:

Posted Date: December 22nd, 2021

DOI: https://doi.org/10.21203/rs.3.rs-1154768/v1

Version of Record: A version of this preprint was published at Nature Communications on February 2nd, 2023. See the published version at https://doi.org/10.1038/s41467-023-36160-5.

Abstract

Engineered T cells transiently expressing tumor-targeting receptors are an attractive form of engineered T cell therapy as they carry no risk of insertional mutagenesis or long-term adverse side-effects. However, multiple rounds of treatment are often required, increasing patient discomfort and cost. To mitigate this, we sought to improve the antitumor activity of transient engineered T cells by screening a panel of small molecules targeting epigenetic regulators for their effect on T cell cytotoxicity. Using a model for engineered T cells targetting hepatocellular carcinoma, we found that short-term inhibition of G9a/GLP increased T cell antitumor activity in *in vitro* models and an orthotopic mouse model. G9a/GLP inhibition increased granzyme expression without terminal T cell differentiation or exhaustion and resulted in specific changes in expression of genes and proteins involved in pro-inflammatory pathways, T cell activation and cytotoxicity.

Introduction

Adoptive cell transfer (ACT) has been highly effective in targeting certain refractory cancers and remains potentially effective for other cancers as new targets of cancer-immune interactions are revealed [1]. ACT involves isolating immunocompetent cells from cancer patients, expanding them *ex vivo*, and infusing them back into the patient. Cells used for ACT can be unmodified tumor-infiltrating lymphocytes (TILs) isolated from the patient or effector cells, typically T cells, isolated from the patient's peripheral blood then engineered to target the tumor by incorporating a T cell receptor (TCR) or chimeric antigen receptor (CAR), with additional modifications to improve immune cell proliferation and persistence [2].

While cell therapies for various lymphomas have led to dramatic tumor regressions and have FDA approval, response in solid tumours remains varied. Solid tumors present unique challenges, such as tumor heterogeneity and the lack of tumor-specific targets, but also an immunosuppressive tumor microenvironment (TME) characterised by poor T cell infiltration and terminal T cell differentiation and exhaustion at the tumor [3]. To overcome the hostile TME, lymphodepleting regimens combined with infusion of large numbers of the T cells is often used [3]. However, introducing large numbers of T cells significantly increases the risk of on-target/off-target toxicity, neurotoxicity, and cytokine release syndrome [1,4]. The use of engineered T cells that transiently express TCRs or CARs by mRNA gene transfer, reduces these risks. Additionally, they avoid the use of viral vectors, hence there is no risk of insertional mutagenesis and can be manufactured more easily at low cost and on a larger scale [5]. Such transient engineered T cells have shown significant antitumor activity in a phase I clinical trial [6] and in preclinical animal models [7,8]. However, multiple infusions are often required, increasing patient discomfort and treatment cost. To minimise this, strategies to improve the antitumor activity of transient engineered T cells are required.

Using small molecule inhibitors is a simple and cost-effective method for modulation of T cell behavior and cell therapy efficacy [9], and has been shown to limit terminal differentiation and promote proliferation

when used during engineered T cell production [10–14]. T cell subpopulations are transcriptionally regulated, and such rapid and precise differentiation is thought to be epigenetically controlled [15,16]. Epigenetic inhibitors are a unique class of small molecule inhibitors with the potential to induce heritable changes in the epigenome and therefore persistent change in T cell behaviour [16]. In this study, we screened a panel of epigenetic inhibitors for their effect on T cell cytotoxicity when added during *ex vivo* T cell expansion, using a model for transient TCR-T cells targeting hepatocellular carcinoma (HCC) [7]. We found that short-term G9a/GLP inhibition during the production of transiently engineered T cells improved antitumor cytotoxicity.

Results

G9a/GLP inhibitors improve the cytotoxicity of TCR-engineered T cells

Engineered transient-expressing TCR^+ T cells have previously been shown to be effective against hepatitis B virus-positive (HBV^+) hepatocellular carcinoma [7]. We therefore used this model to screen for small molecule inhibitors targeting epigenetic regulators that could increase TCR^+ T cell cytotoxicity (Figure 1A). T cells derived from healthy donors were isolated and treated with drugs for 5 days, in accordance with existing clinical practices for expanding patient T cells for T cell therapy [7]. After drug treatment, T cells were transfected with HBV envelope S183–191-specific TCR mRNA by electroporation to generate TCR^+ T cells. TCR^+ T cell toxicity against the target cell line, HepG2-preS1, was evaluated with 2D CellTox™ assays. From 24 pre-selected small molecule inhibitors, 8 increased TCR^+ T cell cytotoxicity by more than 50% (Figure 1B), with A366 resulting in the highest increase (83% relative cytotoxicity). A366 is a selective inhibitor of G9a/GLP [17], a hetero or homodimeric enzyme mainly responsible for mono- and di-methylation of lysine 9 of histone H3 (H3K9me1/2) [18,19].

To confirm the effect of G9a/GLP inhibition on T cell viability and cytotoxicity, we selected two other chemically distinct compounds that selectively inhibit G9a/GLP, UNC0638 [20] and UNC0642 [21]. We identified a concentration that did not affect T cell proliferation (Supplementary Figure 1A), and resulted in effective inhibition of G9a/GLP activity, as assessed by a reduction of H3K9me2 levels (Supplementary Figure 1B-C). We observed a greater decrease in H3K9me2 levels in UNC0638-treated T cells, consistent with previous reports of its higher IC_{50} [20]. TCR^+ T cell cytotoxicity after treatment with the 3 different drugs was evaluated using a previously described 3D microfluidic device assay [22] (Figure 1C). Briefly, HepG2-preS1 cells were seeded in a collagen matrix in microfluidic channels, and TCR^+ T cells were introduced into one channel and allowed to migrate into the matrix toward target cells, and the proportion of target cells killed by T cells was quantified after 24 h. While TCR^+ T cell cytotoxicity generally improved after G9a/GLP inhibition, TCR^+ T cell cytotoxicity did not improve for some donors with UNC0638 and A366 (Figure 1C). UNC0642-treated T cells showed the most consistent and greatest increase in target

cell killing (Figure 1C). UNC0642 also has a better pharmacokinetic profile than UNC0638 or A366 [21]; hence, UNC0642 was used in further experiments.

To verify the effect of UNC0642 treatment and account for donor-dependent variation, we repeated the 2D and 3D cytotoxicity assays with additional donors (Figure 1D-J). TCR^+ T cell cytotoxicity was assayed in 2D in real time during co-culture with target cells using the xCELLigence® RTCA DP (Figure 1D-F). By 48 h, TCR^+ T cells (blue, Figure 1D) restricted HepG2-preS1 cell growth more than mock electroporated TCR^- T cells (purple, Figure 1D), indicating that expression of the transfected TCR improved T cell targeting and cytotoxicity as previously reported [7]. UNC0642 treatment of TCR^+ T cells (red, Figure 1D) further increased T cell cytotoxicity, with a dramatic decrease in target cell number observed at approximately 40 h. Electroporated TCR^+ T cells lose most of their TCR expression at 72 h post-electroporation (Figure 1G, Supplementary Figure 1D) [7], but UNC0642 treatment did not affect TCR expression (Supplementary Figure 1E). UNC0642-treated TCR^+ T cells sustained an increase in cytotoxicity compared to untreated T cells over at both 48 h (Figure 1E) and 72 h (Figure 1F).

Using the 3D cytotoxicity assay, we evaluated both the cytotoxicity and migration of TCR^+ T cells (Figure 1H-J). Similar to our observations in 2D, TCR expression improved target cell killing in 3D, and UNC0642-treated TCR^+ T cells resulted in increased target cell killing (Figure 1I). UNC0642 treatment did not increase cytotoxicity of TCR^- T cells or naïve T cells (Figure 1I). TCR expression improved T cell migration into the collagen matrix (Figure 1J), however there was no difference in T cell migration for UNC0642-treated TCR^+ T cells, suggesting that UNC0642 treatment increases the intrinsic cytotoxicity of T cells rather than their ability to migrate.

Overall, the data indicate that G9a/GLP inhibition during T cell expansion increases TCR^+ T cell target cell killing efficiency by increasing cytotoxicity.

The G9a/GLP inhibitor UNC0642 increases the expression of markers of T cell activation and effector function without affecting T cell subpopulations

Epigenetic factors regulate T cell differentiation potential and phenotype [23], and T cell subpopulations such as $CD8^+$ and cytotoxic $CD4^+$ cells are associated with target cell killing. We therefore investigated if our observed change in T cell cytotoxicity was associated with different T cell subpopulations. UNC0642 treatment did not affect $CD4^+$ and $CD8^+$ proportions (Figure 2A, Supplementary Figure 2A). We also did not observe any changes in distinct $CD4^+$ T cell subpopulations (Treg, Th1, Th2, and Th17) (Supplementary Figure 2B), $CD4^+$ memory subtypes (Supplementary Figure 2C) or $CD8^+$ memory subtypes (Supplementary Figure 2D).

Increased T cell cytotoxicity is also linked to terminal differentiation of effector T cells, and subsequent deterioration of T cell function, or T cell exhaustion [24]. We therefore investigated T cell activation and exhaustion after UNC0642 treatment (Figure 2B-C). UNC0642 treatment resulted in a significant increase

in granzyme B (GzmB) and small increase in Interleukin-2 (IL-2) expression while there were no changes in Perforin (Perf), Interferon gamma (IFNγ) and Tumour Necrosis Factor alpha (TNFα) expression (Figure 2A). UNC0642 treatment also led to a small increase in the expression of Programmed Cell Death protein 1 (PD1) and CD39 but had no effect on Cytotoxic T-Lymphocyte Associated Protein 4 (CTLA4), Lymphocyte Activating Gene 3 (LAG3) or T-cell Immunoglobulin domain and Mucin domain 3 (TIM3) expression (Figure 2C). Because $CD4^+$ and $CD8^+$ T cells play different roles in T cell cytotoxicity, and UNC0642 might differentially affect these subpopulations, we further assessed activation and exhaustion markers in these two populations (Figure 2D-E). UNC0642 treatment increased GzmB expression dramatically in CD4+ and CD8+ T cells, while we observed a lesser increase in IFNγ, TNFα and IL2 expression that was not significant due to donor-dependent variability (Figure 2D). We observed a small increase in CTLA4 expression in $CD4^+$ T cells, and small increases in PD1, CTLA4 and CD39 expression in $CD8^+$ T cells.

T cell terminal differentiation and exhaustion are proposed occur in a multi-step process induced by T cell activation, and expression of activation markers can overlap with exhaustion markers alone [25]. This is consistent with our observations, in which T cell cytotoxicity and effector markers (GzmB and IL2) were upregulated simultaneously with some markers of activation/exhaustion (PD1 and CD39). To more accurately simulate T cell activation and exhaustion, we investigated the effect of UNC0642 on $CD4^+$ and $CD8^+$ T cell GzmB, PD1, CTLA4, CD39 and TIM3 expression when TCR^+ T cells were co-cultured with HepG2-preS1 target cells for up to 48 h, which is within the window of TCR^+ T cell cytotoxicity (Figure 1D-I). Measurements were taken just after UNC0642 treatment/ before TCR transfection (-48 h from co-culture), 24 h after transfection (-24 h), and 24 h or 48 h after co-culture with target cells (Figure 2F-G, Supplementary Figure 2E-H). GzmB expression in $CD4^+$ and $CD8^+$ T cells increase after TCR transfection, and increased further after co-culture with target cells, peaking at 24 h (Figure 2F-G). UNC0642 treatment resulted in a higher expression of GzmB in both populations of T cells before (-48 h) and after TCR transfection (-24 h) (Figure 2F-G). This increase was sustained in $CD8^+$ T cells after 24 h of co-culture with target cells (Figure 2G). PD1 expression levels were unchanged for $CD4^+$ T cells, while they increased after co-culture for $CD8^+$ T cells (Supplementary Figure 2E). However, UNC0642 treatment did not affect PD1 expression in these cells (Supplementary Figure 2E). CTLA4 expression increased to a lesser degree in $CD4^+$ and $CD8^+$ T cells, and we observed a small increase in CTLA4 expression in UNC0642-treated $CD4^+$ T cells before co-culture (Supplementary Figure 2F). CD39 and TIM3 expression remained relatively unchanged for $CD4^+$ T cells, while their expression increased after co-culture for $CD8^+$ T cells (Supplementary Figure 2G-H). However, their expression after UNC0642 treatment was not dramatically increased in $CD4^+$ or $CD8^+$ T cells (Supplementary Figure 2G-H).

Taken together, the data suggested that UNC0642 treatment increases T cell cytotoxicity by increasing GzmB expression, without modifying T cell subpopulations or T cell activation or exhaustion.

The G9a/GLP inhibitor UNC0642 changes chemokine expression and cytotoxicity pathways at the transcriptional

level

Because UNC0642 inhibits the epigenetic regulator G9a/GLP, to understand the impact of UNC0642 at the genetic level, we conducted a targeted genomics screen using the NanoString nCounter CAR-T characterization gene expression panel that assays 770 genes known to be involved in T cell activation, exhaustion, metabolism, persistence, toxicity and phenotype. UNC0642 treatment resulted in differential expression of various chemokines (upregulated: *CCL18, CCL23, CCL1, CXCL8, XCL1/2*, and downregulated: *CX3CR1*) as well as genes related to T cell costimulatory activity (upregulated: *CTLA4*) and exhaustion (upregulated: *FOXP3*) (Figure 3A, Supplementary Figure 3A). Increased transcription of *CCL18*, *CCL23*, and *CCL1* was validated by qPCR (Figure 3B). Additionally, we determined by ChIP-qPCR that levels of H3K9me2, a key G9a/GLP target and regulator of transcription, at *CCL18* and *CCL23* were significantly decreased (Figure 3C). Increase in *CCL18* expression at the translational level was confirmed by ELISA (Figure 3D and 3E).

Using the NanoString nSolver analysis platform, we observed that UNC0642 treatment increased the expression of genes associated with the Th2 pathway, cytotoxicity, innate-like T cells, Th17 and Treg signaling and glycolysis (Figure 3F). By contrast, the expression of genes related to the Th1 pathway and type II interferon signaling was decreased (Figure 3F). These results are consistent with our flow cytometry data suggesting that UNC0642 treatment increases T cell cytotoxicity to a large degree and activation to a smaller degree (Figure 2A-B). Changes to cellular metabolism were also suggested in the Nanostring data, hence the mitochondrial and glycolytic capacity of T cells after UNC0642 treatment was analysed by extracellular flux. We found that UNC0642 treatment increased the maximum mitochondrial respiration and spare capacity of T cells (Figure 3G), indicating that oxidative phosphorylation was increased. UNC0642 treatment did not affect the glycolytic profile of T cells (Figure 3H). Exhausted T cells suppress mitochondrial respiration and glycolysis, while effector T cells rely mainly on aerobic glycolysis to produce energy [25]. We observe an increase in mitochondrial respiration and no changes in glycolysis after UNC0642 treatment, which is consistent with our flow cytometry data showing that UNC0642 treatment increased the expression of effector T cell markers, but not not exhaustion markers (Figure 2A-B and Supplementary Figure 2F-G). Overall, the data indicate that UNC0642 is affecting the expression of specific genes related to T cell effector function, such as cytotoxicity, activation and mitochondrial respiration.

Proteins associated with T cell activation and cytotoxicity are increased after UNC0642 treatment

To fully characterise the effect of UNC0642 on T cells and to account for possible post-transcriptional modifications, we performed a high-throughput proteomic screen with quantitative proteomics using tandem mass tags (TMT). Briefly, T cells were treated with UNC0642, and samples from treated and untreated T cells were collected every 24 h until day 5. Protein samples were labeled using distinct TMT tags and the protein abundance was determined by comparing treated and untreated T cells over time. A total of 4,918 proteins were identified and quantified; of these, 2,243 (approximately 45%) were identified

on all 5 days. Only a small number of proteins exhibited changes in abundance (log2 fold change ± 0.5, $P \leq 0.05$) over time in UNC0642-treated T cells compared to untreated T cells (6, 22, 10, 15 and 7 on days 1–5, respectively) (days 1–4: Supplementary Figure 4A-D and day 5: Figure 4A). On day 1, we observed an increase in proteins involved in gene regulation such as zinc finger protein 587B (ZNF587B) and primase and DNA directed polymerase (PRIMPOL), as well as lysosomal protein transmembrane 5 (LAPTM5), Interleukin 32 (IL32) and Serine Incorporator 1 (SERINC1) (Supplementary Figure 4A). On Day 2, we observed increases in proteins involved in post-translational protein modification and regulation such as DnaJ Heat Shock Protein Family (Hsp40) Member C10 (DNAJC10), G Protein-Coupled Receptor Associated Sorting Protein 2 (GPRASP2), Ankyrin Repeat Domain 28 (ANKRD28), and ST3 Beta-Galactoside Alpha-2,3-Sialyltransferase 3 (ST3GAL3); as well as increases in proteins involved in gene expression regulation such as TMF1 Regulated Nuclear Protein 1 (TRNP1) and CCHC-Type Zinc Finger Nucleic Acid Binding Protein (CNBP) (Supplementary Figure 4B). On Day 3, there was an increase in Mediator Complex Subunit 1 (MED1), involved in gene transcription, and Dishevelled Associated Activator Of Morphogenesis 1 (DAAM1), involved in Wnt and Rho signalling, as well as an increase in proteins associated with the lysosomal pathway – LAPTM5, NPC Intracellular Cholesterol Transporter 2 (NPC2) and Serpin Family B Member 6 (SERPINB6) (Supplementary Figure 4C). On day 4, we observed an enrichment for granzyme B, proteins involved in immune cell signalling – Major Histocompatibility Complex, Class II, DR Alpha (HLA-DR), HCLS1 Binding Protein 3 (HS1BP3), Immunoglobulin Lambda Constant 2 (IGLC2), Immunoglobulin Lambda Like Polypeptide 5 (IGLL5) (Supplementary Figure 4D).

On the last day of UNC0642 treatment, granzymes B and H (GZMB, GZMH), lysosomal-associated membrane protein 1 (LAMP-1), macrophage-capping protein (CAPG) and epididymal secretory protein E1 (NCP2) were significantly upregulated, while only DEAD-box helicase 54 (DDX54) was downregulated (Figure 4A). GO enrichment of the top 50 upregulated proteins revealed functions related to processes including immune response, cell activation and cell killing, while GO enrichment of downregulated proteins showed only a small enrichment in metabolic processes (Figure 4B). We validated the changes in expression of GZMB and GZMM, and confirmed an increase after UNC0642 treatment, and perforin expression, which did not increase significantly (Figure 4C). Notably, the degree of change detected by flow cytometry matched that detected in the proteomics analysis, providing additional confidence in the validity of the hits (Figure 4C).

To identify trends in protein abundance over the 5 days of UNC0642 treatment, unsupervised k-means clustering was applied to the 2,243 proteins identified across all 5 days, resulting in 10 different clusters with similar abundance profiles during UNC0642 treatment (Figure 4D and Supplementary Figure 4E). Majority of proteins were classified in clusters with a transient change in abundance (clusters 5, 6, 7 and 10, Supplementary Figure 4E) or no change over the 5 days (clusters 1, 2, 3 and 9, Supplementary Figure 4E). By contrast, proteins in cluster 8 had an increased abundance while proteins in cluster 4 had a slight decrease in abundance. Proteins that were upregulated at day 5 (Figure 4A) were identified in cluster 8 (GZMB, CAPG, GZMM, NCP2, GZMH) (Figure 4D), indicating a sustained increase in the expression of these proteins during treatment. GO analysis of the proteins in cluster 8 showed enrichment in immune response, immune cell activation and effector processes (Figure 4E), while proteins with slightly

decreased expression in cluster 4 were enriched in metabolic processes (Figure 4E). Overall, the data indicate that UNC0642 treatment affects T cell behavior at the protein level, with a sustained increase in proteins associated with T cell activation and cytotoxicity. Additionally, the data suggest that UNC0642 treatment triggers early changes in proteins involved in gene expression and post-translational protein modification and regulation, and later changes in proteins in the lysosomal pathway and T cell signalling.

UNC0642 treatment improves engineered TCR+ T cell antitumor activity in an orthotopic mouse model of HCC

Given the encouraging data for engineered T cells *in vitro*, we next examined the ability of UNC0642 treatment to increase the cytotoxicity of transient engineered TCR^+ T cells *in vivo*. We established an orthotopic xenograft model in NSG mice by intrahepatic injection of HepG2-2.2.15 target cells expressing luciferase, to better recapitulate the T cell targeting and cytotoxicity to the liver than in a subcutaneous xenograft model. One week later, intravenous injection of untreated or UNC0642-treated TCR^+ T cells on alternate days were administered for a total of five injections (Figure 5A) and the tumor burden was monitored by *in vivo* bioluminescence imaging (IVIS) (Figure 5B). We observed a significant reduction in tumor growth in mice injected with UNC0642-treated TCR^+ T cells (red) compared to mice injected with untreated TCR^+ T cells (blue) or not treated with T cells at all (green) at day 18 post-tumor injection (Figure 5B-C). Mice injected with UNC0642-treated TCR^+ T cells also had less weight loss than mice in the other two groups (Figure 5D). It is worth noting that mice injected with untreated TCR^+ T cells had a similar tumor growth rate and weight loss to mice with no T cells injected (compare blue and green, Figure 5C). One possibility might be that the immune-tolerant environment of the liver inhibits T cell infiltration and cytotoxicity [26]. Histological analysis confirmed that injected TCR^+ T cells were appropriately targeting the liver tumor in mice receiving untreated or UNC0642-treated TCR^+ T cells (Figure 5E), suggesting that increased antitumor activity in UNC0642-treated T cells is due to increased T cell cytotoxicity rather than T cell targeting. This is consistent with our *in vitro* 3D cytotoxicity assays (Figure 1I-J). Additionally, the data suggest that UNC0642 treatment improves engineered TCR^+ T cell ability to overcome immunosuppressive environments.

UNC0642 treatment improves the cytotoxicity of patient-derived TCR-T cells, CAR-T and NK cells

Engineered TCR^+ T cells used in the clinic are usually generated by modifying T cells obtained from patients, which may have impaired cytotoxicity due to prolonged tumor progression or chemotherapy [27]. We therefore investigated the ability of UNC0642 treatment to improve engineered TCR^+ T cells generated from patients diagnosed with HBV-related HCC. T cells were isolated from blood from two HBV-related HCC patients, and processed in the same way as those obtained from healthy donors (Figure 6A). UNC0642 treatment increased expression of granzymes B and M and perforin (Figure 6B, Supplementary Figure 5A). In Patient 1, UNC0642 treatment did not result in any significant changes in target cell lysis compared with the untreated T cells in the 2D or 3D cytotoxicity assays (top panel, Figure 6C-D). By

contrast, in Patient 2 UNC0642 treatment resulted in a dramatic increase in target cell death compared to untreated TCR^+ T cells (bottom panel, Figure 6C-D). Notably, TCR^+ T cells were much more efficient at target cell killing than TCR- T cells in Patient 1 (compare pink and blue lines in Figure 6C, TCR^- and TCR^+ blue points in Figure 6D), suggesting that the impact of UNC0642 treatment on cytotoxicity might be masked by the efficiency of TCR engineering in this patient. T cell migration into the 3D matrix was also higher for Patient 1 than Patient 2 (Figure 6E), and UNC0642 treatment did not affect T cell migration.

T cells stably-expressing chimeric antigen receptors (CARs) are also an important adoptive cell therapy product with synthetic immunoreceptors that specifically target cancer cells [28]. We investigated the effect of UNC0642 on CAR-T cells targeting CD133 (Figure 6E), expressed by cancer stem cells originating from various epithelial cells [29], including the liver cancer cell line Hep3B (99.6% $CD133^+$) (Supplementary Figure 5B). UNC0642 treatment significantly increased the production of granzymes B and M and perforin in CAR-T cells (Figure 6F, Supplementary Figure 5C). In functional killing assays, untreated CAR-T cells exhibited remarkable target cell lysis, and UNC0642 treatment improved CAR-T cell cytotoxicity slightly (Figure 6G-H), and there was no observable difference at day 3 of the 3D cytotoxicity assay (Figure 6H). There was also an increase in CAR-T cell migration in the 3D matrix from day 2 to day 3, suggesting that as more CAR-T cells migrate towards the target cells, their effective cytotoxicity increases such that the increase in granzymes due to UNC0642 did not drive further target cell killing.

To assess whether UNC0642 treatment might also increase granzyme expression and cytotoxicity in other cytotoxic cell types, we evaluated the effect of UNC0642 on NK cells. NK cells play a critical role in immune activation against abnormal cells, including cancer cells and perform an essential function in tumor immunosurveillance [30]. NK cells were isolated from four different donors and treated for 5 days with UNC0642 (Figure 6J). UNC0642 treatment significantly increased the levels of granzymes B and M and perforin in NK cells from all four donors compared to the untreated NK cells (Figure 6I, Supplementary Figure 5D), suggesting an increase in the NK cytotoxicity similar to the increase observed in T cells. Accordingly, UNC0642 treatment increased NK cell cytotoxicity in a 2D cytotoxic assay (Figure 6J). Overall, G9a inhibition appears to increase granzyme expression and antitumor cytotoxicity of multiple engineered and innate cytotoxic cell types.

Discussion

Transient engineered TCR^+ T cells are a valuable and effective antitumour therapy, while also carrying low to no risk of cytokine release syndrome or insertional mutagenesis. However, their transient nature does mean they have a shorter window of antitumour activity and multiple infusions are required, and so there is a need to improve their efficacy further to minimise patient cost and discomfort. By screening small molecules that regulate epigenetic players, we have exploited epigenetic T cell regulation to improve the cytotoxicity of transient engineered TCR^+ T cells. We found that low-dose inhibition of G9a/GLP by UNC0642 treatment of T cells during their *ex vivo* expansion phase resulted in increased T cell cytotoxicity in multiple *in vitro* and *in vivo* assays. This increase in cytotoxicity is likely due to an

increase in granzyme expression, especially GZMB. Interestingly, G9a/GLP inhibition during cell expansion protocols increased the granzyme expression and cytotoxic capability of TCR-engineered T cells (from healthy and patient donors), CAR-T cells and NK cells, suggesting that G9a/GLP is involved in granzyme expression and cytotoxicity across multiple cytotoxic immune cell types.

G9a/GLP has been reported to regulate immune cell differentiation and functions [23], such as type II cytokine production [31], and Th17/ Treg differentiation [32]. In accordance with this, our targeted genomics screen revealed changes in genes related to Th2, Th17 and Treg cells. However, we did not detect any changes to the T cell sub-populations after UNC0642 treatment during the expansion phase. It is likely that while UNC0642 treatment at 1.25 μM for 5 days was sufficient to reduce H3K9me2 levels by approximately 50%, this dose was insufficient to result in the re-programming of T cells observed in other studies in where knock-out models or higher pharmacological doses were used. Additionally, most studies investigated the role of G9a/GLP on naïve T cell differentiation, while our study involves differentiated T cells, where the epigenetic landscape is different. In differentiated immune cells, G9a has been implicated in $CD8^+$ effector memory cell persistence [33], as well as macrophage tolerance to chronic endotoxin infection [34–36]. Similarly, our data shows that the antitumor activity of $CD4^+$/$CD8^+$ T cells is improved following G9a/GLP inhibition, due to an increase in T cell cytotoxicity, via an increase in granzyme production, rather than T cell targeting. Notably, the increase in cytotoxicity was not accompanied by characteristic features of T cell exhaustion, such as a decrease in cell proliferation, expression of T cell exhaustion markers, or decreases in mitochondrial respiration and glycolytic capability. Our findings also highlight the importance of using a range of functional assays, such as 3D *in vitro* models and orthotopic *in vivo* models to evaluate T cell effector function, as the expression of activation and exhaustion markers alone was not always indicative of T cell function.

Both genomic and proteomic analyses revealed increases in T cell activation and cytotoxicity, although the same genes were not identified. Discordance between genomic and proteomic profiles are common [35]; however, comparing differentially expressed genes and proteins provides greater confidence in the data [37]. Differences could be due to the read-outs used and changes at the post-transcriptional level. We found that UNC0642 treatment predominantly led to an upregulation of gene or protein levels, which is consistent with the canonical role of G9a/GLP as an epigenetic repressor. Previous studies where G9a was silenced in germ cells found only eight genes upregulated by more than 2-fold, despite significant loss of H3K9me2/1 [38]. We observed a similar phenomenon, where G9a reduction by UNC0642 treatment affected only a handful of genes and proteins. G9a/GLP has also been reported to regulate methylation of non-histone targets, including G9a itself [23]; hence changes in cell behavior may be induced by changes in protein interactions rather than through changes at the genetic or protein level. Our targeted genomics screen revealed significant changes in chemokine expression after UNC0642, most significantly of which was CCL18. CCL18 is a chemoattractant for naïve T cells, T and B lymphocytes and NK cells [39]. CCL18 is also predominantly produced by M2 macrophages and TAMs, and can induce the differentiation of effector T cells into Tregs [40]. CCL18 can also promote cancer cell invasion by inducing epithelial-mesenchymal transition (EMT) [41–45]. In our study, Treg subpopulations were unchanged following

UNC0642 treatment, and we did not observe an increase in the tumor invasive front in our *in vivo* model following the transfer of UNC0642-treated T cells. Given that post-translational modifications can significantly modify chemokine activity [46] and their effects can be highly context-dependent, further research is needed into the functional role of CCL18 and other cytokines involved in T cell cytotoxicity and their regulation by G9a/GLP.

Our proteomic screen revealed an increase immune effector process, and confirmed an upregulation in proteins involved in the granzyme-mediated apoptotic signalling pathway. We observed early changes in proteins involved in gene expression, followed by changes in protein post-translational modifications, followed by changes in proteins involved in the lysosomal pathway, T cell signalling and granzyme production. The data suggests that UNC0642 is acting upon the granzyme production pathway by triggering a molecular cascade, starting with gene expression. Blimp1/G9a has been suggested to negatively regulate Granzyme B expression [33]. Although changes in Blimp1 were not found in our study, our data suggests a similar role of G9a/GLP in suppressing granzyme expression in effector T cells. Further studies involving the proteins we found differentially regulated in our screen and possible interactions with Blimp1 are warranted.

We demonstrated that G9a/GLP improved cytotoxicity in a range of cytotoxic cell types – TCR-engineered T cells from healthy and patient donors; CAR-T cells, as well as NK cells. This suggests that G9a/GLP-regulated H3K9me2 may be involved in a general mechanism that underlies the repression of cytotoxicity-related genes in terminally differentiated T cells and NK cells. Consistent with this, a general consensus is emerging whereby immune cell differentiation is associated with progressive increases in epigenetic repressive markers, such as H3K9me2 or H3K9me3 [47]. Epigenetic regulation results in heritable changes in T cell behavior; however, we did not evaluate long-term T cell cytotoxicity and epigenetic changes. Additionally, it would be interesting to see if UNC0642 treatment has a similar effect on other cytolytic immune cell types, such as lymphokine-activated killer (LAK) cells.

In conclusion, we show that the use of a small molecule inhibitor of an epigenetic regulator, G9a/GLP, during *ex vivo* expansion is a convenient and effective method of improving the cytotoxicity of transiently engineered TCR-T cells, as well as other cytotoxic cell types such as CAR-T cells and NK cells, via increase of granzyme secretion. Notably, the increase in T cell cytotoxicity was able to overcome the immunosuppressive environment of solid tumors in an orthotopic model of HCC. G9a/GLP inhibition resulted in specific changes at the genetic and protein levels, and further research is required to fully elucidate the role of G9a/GLP in cytotoxic cell types. Overall, our results add to a growing body of evidence that supports epigenetic modulation of ACT products to improve antitumor efficiency, which in turn, could reduce the risk of adverse side-effects and the cost of ACT.

Materials And Methods

Study design

The objective of this study was to evaluate the potential therapeutic effect of small molecule inhibitors on T cells during *ex vivo* expansion. A panel of small molecule inhibitors was screened using the CellTox™ cytotoxicity assay. After selection of the G9a/GLP inhibitor UNC0642 using different 2D and 3D assays, a wide range of *in vitro and in vivo* assays were performed to confirm the efficacy of UNC0642 in boosting the cytotoxicity of T cells against cancer cells. For *in vitro* studies, at least three independent experiments were carried out, and in the case of primary cells isolated from blood, at least three donors were tested unless otherwise indicated. NOD-SCID-IL2RGnull (NSG) mice (aged 8–10 weeks) were used for in vivo experiments, with 5 to 10 mice per group to ensure statistical power. Mice were euthanized humanely at defined study endpoints, and all experimental procedures were approved by the Institutional Animal Care and Use Committee (IACUC) of A*STAR (Biopolis, Singapore) (IACUC No. 18139) in accordance with the guidelines of the Agri-Food & Veterinary Authority (AVA) and the National Advisory Committee for Laboratory Animal Research (NACLAR). The same effect was observed in NK cells and CAR-T cells and also in TCR-engineered T cells isolated from patients diagnosed with HBV-related HCC HCC (IRB: NUS-IRB H17-023E).

Declarations

ACKNOWLEDGEMENTS

We want to thank Alrina Shin Min Tan for her help with the Seahorse experiments and Winnie Teo for supporting the mRNA production. Also, We want to thank Ginny Xiaohe Li for the support with the proteomic analysis and thanks to Christine Tham for her support with the Nanostring experiments.

Funding:

This work was supported by the Open Fund - Young Individual Research Grant (OF-YIRG) - OFYIRG18nov-0002, NRF-CRP17-2017-06; Singapore National Research Foundation, NRF-SIS “SingMass” grant to R.M.S and by the Institute of Molecular and Cell Biology, Agency for Science Technology and Research (A*STAR), Singapore.

Author contributions:

AP, GA, MSYL, JARC and JRO designed the experiments. MSYL, JARC, JRO, JA and DT performed the experiments, EC and TT helped with some experimental procedures. YTL, WLC and RMS performed the proteomic analysis. AB, EG and AP were involved in conceptualize the work and funding acquisition. All authors participated in the writing of the manuscript and approved the final version.

Competing interests:

A.P. is a consultant and shareholder of AIM Biotech Pte. Ltd.; E.G. and T.T. are cofounders and scientific advisors of IMMUNOA Pte Ltd. T.T. is in the Board of Directors of IMMUNOA Pte Ltd; A.B. is cofounder of

Lion TCR Pte Ltd, in the Board of Directors Lion TCR Pte Ltd and in the Board of Directors of IMMUNOA Pte Ltd; E.G. has served on advisory board for Lion TCR Pte Ltd.

Data and materials availability:

All data associated with this study are present in the paper or the Supplementary Materials.

References

1. Leko, V. & Rosenberg, S. A. Identifying and Targeting Human Tumor Antigens for T Cell-Based Immunotherapy of Solid Tumors. *Cancer Cell* **38**, 454–472, doi:10.1016/j.ccell.2020.07.013 (2020).
2. Li, D. *et al.* Genetically engineered T cells for cancer immunotherapy. *Signal Transduct Target Ther* **4**, 35, doi:10.1038/s41392-019-0070-9 (2019).
3. Baruch, E. N., Berg, A. L., Besser, M. J., Schachter, J. & Markel, G. Adoptive T cell therapy: An overview of obstacles and opportunities. *Cancer* **123**, 2154–2162, doi:10.1002/cncr.30491 (2017).
4. Morris, E. C., Neelapu, S. S., Giavridis, T. & Sadelain, M. Cytokine release syndrome and associated neurotoxicity in cancer immunotherapy. *Nat Rev Immunol*, doi:10.1038/s41577-021-00547-6 (2021).
5. Kowalski, P. S., Rudra, A., Miao, L. & Anderson, D. G. Delivering the Messenger: Advances in Technologies for Therapeutic mRNA Delivery. *Mol Ther* **27**, 710–728, doi:10.1016/j.ymthe.2019.02.012 (2019).
6. Zhao, Y. *et al.* Multiple injections of electroporated autologous T cells expressing a chimeric antigen receptor mediate regression of human disseminated tumor. *Cancer Res* **70**, 9053–9061, doi:10.1158/0008-5472.CAN-10-2880 (2010).
7. Koh, S. *et al.* A practical approach to immunotherapy of hepatocellular carcinoma using T cells redirected against hepatitis B virus. *Mol Ther Nucleic Acids* **2**, e114, doi:10.1038/mtna.2013.43 (2013).
8. Pohl-Guimaraes, F., Hoang-Minh, L. B. & Mitchell, D. A. RNA-electroporated T cells for cancer immunotherapy. *Oncoimmunology* **9**, 1792625, doi:10.1080/2162402X.2020.1792625 (2020).
9. van der Zanden, S. Y., Luimstra, J. J., Neefjes, J., Borst, J. & Ovaa, H. Opportunities for Small Molecules in Cancer Immunotherapy. *Trends Immunol* **41**, 493–511, doi:10.1016/j.it.2020.04.004 (2020).
10. Sabatino, M. *et al.* Generation of clinical-grade CD19-specific CAR-modified CD8+ memory stem cells for the treatment of human B-cell malignancies. *Blood* **128**, 519–528, doi:10.1182/blood-2015-11-683847 (2016).
11. Klebanoff, C. A. *et al.* Inhibition of AKT signaling uncouples T cell differentiation from expansion for receptor-engineered adoptive immunotherapy. *JCI Insight* **2**, doi:10.1172/jci.insight.95103 (2017).
12. Bowers, J. S. *et al.* PI3Kdelta Inhibition Enhances the Antitumor Fitness of Adoptively Transferred CD8(+) T Cells. *Front Immunol* **8**, 1221, doi:10.3389/fimmu.2017.01221 (2017).

13. Bae, J. *et al.* Histone deacetylase (HDAC) inhibitor ACY241 enhances anti-tumor activities of antigen-specific central memory cytotoxic T lymphocytes against multiple myeloma and solid tumors. *Leukemia* **32**, 1932–1947, doi:10.1038/s41375-018-0062-8 (2018).
14. Wang, Y. *et al.* Low-dose decitabine priming endows CAR T cells with enhanced and persistent antitumour potential via epigenetic reprogramming. *Nat Commun* **12**, 409, doi:10.1038/s41467-020-20696-x (2021).
15. Henning, A. N., Roychoudhuri, R. & Restifo, N. P. Epigenetic control of CD8(+) T cell differentiation. *Nat Rev Immunol* **18**, 340–356, doi:10.1038/nri.2017.146 (2018).
16. Tough, D. F., Rioja, I., Modis, L. K. & Prinjha, R. K. Epigenetic Regulation of T Cell Memory: Recalling Therapeutic Implications. *Trends Immunol* **41**, 29–45, doi:10.1016/j.it.2019.11.008 (2020).
17. Sweis, R. F. *et al.* Discovery and development of potent and selective inhibitors of histone methyltransferase g9a. *ACS Med Chem Lett* **5**, 205–209, doi:10.1021/ml400496h (2014).
18. Ogawa, H., Ishiguro, K., Gaubatz, S., Livingston, D. M. & Nakatani, Y. A complex with chromatin modifiers that occupies E2F- and Myc-responsive genes in G0 cells. *Science* **296**, 1132–1136, doi:10.1126/science.1069861 (2002).
19. Tachibana, M. *et al.* Histone methyltransferases G9a and GLP form heteromeric complexes and are both crucial for methylation of euchromatin at H3-K9. *Genes Dev* **19**, 815–826, doi:10.1101/gad.1284005 (2005).
20. Vedadi, M. *et al.* A chemical probe selectively inhibits G9a and GLP methyltransferase activity in cells. *Nat Chem Biol* **7**, 566–574, doi:10.1038/nchembio.599 (2011).
21. Liu, F. *et al.* Discovery of an in vivo chemical probe of the lysine methyltransferases G9a and GLP. *J Med Chem* **56**, 8931–8942, doi:10.1021/jm401480r (2013).
22. Pavesi, A. *et al.* A 3D microfluidic model for preclinical evaluation of TCR-engineered T cells against solid tumors. *JCI Insight* **2**, doi:10.1172/jci.insight.89762 (2017).
23. Scheer, S. & Zaph, C. The Lysine Methyltransferase G9a in Immune Cell Differentiation and Function. *Front Immunol* **8**, 429, doi:10.3389/fimmu.2017.00429 (2017).
24. Wherry, E. J. & Kurachi, M. Molecular and cellular insights into T cell exhaustion. *Nat Rev Immunol* **15**, 486–499, doi:10.1038/nri3862 (2015).
25. Sakuishi, K. *et al.* Targeting Tim-3 and PD-1 pathways to reverse T cell exhaustion and restore anti-tumor immunity. *J Exp Med* **207**, 2187–2194, doi:10.1084/jem.20100643 (2010).
26. Zheng, M. & Tian, Z. Liver-Mediated Adaptive Immune Tolerance. *Front Immunol* **10**, 2525, doi:10.3389/fimmu.2019.02525 (2019).
27. Xia, A., Zhang, Y., Xu, J., Yin, T. & Lu, X. J. T Cell Dysfunction in Cancer Immunity and Immunotherapy. *Front Immunol* **10**, 1719, doi:10.3389/fimmu.2019.01719 (2019).
28. June, C. H. & Sadelain, M. Chimeric Antigen Receptor Therapy. *N Engl J Med* **379**, 64–73, doi:10.1056/NEJMra1706169 (2018).

29. Wang, Y. *et al.* CD133-directed CAR T cells for advanced metastasis malignancies: A phase I trial. *Oncoimmunology* **7**, e1440169, doi:10.1080/2162402X.2018.1440169 (2018).
30. Lopez-Soto, A., Gonzalez, S., Smyth, M. J. & Galluzzi, L. Control of Metastasis by NK Cells. *Cancer Cell* **32**, 135–154, doi:10.1016/j.ccell.2017.06.009 (2017).
31. Lehnertz, B. *et al.* Activating and inhibitory functions for the histone lysine methyltransferase G9a in T helper cell differentiation and function. *J Exp Med* **207**, 915–922, doi:10.1084/jem.20100363 (2010).
32. Antignano, F. *et al.* Methyltransferase G9A regulates T cell differentiation during murine intestinal inflammation. *J Clin Invest* **124**, 1945–1955, doi:10.1172/JCI69592 (2014).
33. Shin, H. M. *et al.* Epigenetic modifications induced by Blimp-1 Regulate CD8(+) T cell memory progression during acute virus infection. *Immunity* **39**, 661–675, doi:10.1016/j.immuni.2013.08.032 (2013).
34. Chen, X., El Gazzar, M., Yoza, B. K. & McCall, C. E. The NF-kappaB factor RelB and histone H3 lysine methyltransferase G9a directly interact to generate epigenetic silencing in endotoxin tolerance. *J Biol Chem* **284**, 27857–27865, doi:10.1074/jbc.M109.000950 (2009).
35. Liu, C. *et al.* A chromatin activity-based chemoproteomic approach reveals a transcriptional repressome for gene-specific silencing. *Nat Commun* **5**, 5733, doi:10.1038/ncomms6733 (2014).
36. Yoshida, K. *et al.* The transcription factor ATF7 mediates lipopolysaccharide-induced epigenetic changes in macrophages involved in innate immunological memory. *Nat Immunol* **16**, 1034–1043, doi:10.1038/ni.3257 (2015).
37. Koussounadis, A., Langdon, S. P., Um, I. H., Harrison, D. J. & Smith, V. A. Relationship between differentially expressed mRNA and mRNA-protein correlations in a xenograft model system. *Sci Rep* **5**, 10775, doi:10.1038/srep10775 (2015).
38. Tachibana, M., Nozaki, M., Takeda, N. & Shinkai, Y. Functional dynamics of H3K9 methylation during meiotic prophase progression. *EMBO J* **26**, 3346–3359, doi:10.1038/sj.emboj.7601767 (2007).
39. Krohn, S., Garin, A., Gabay, C. & Proudfoot, A. E. The Activity of CCL18 is Principally Mediated through Interaction with Glycosaminoglycans. *Front Immunol* **4**, 193, doi:10.3389/fimmu.2013.00193 (2013).
40. Chang, Y. *et al.* The chemokine CCL18 generates adaptive regulatory T cells from memory CD4+ T cells of healthy but not allergic subjects. *FASEB J* **24**, 5063–5072, doi:10.1096/fj.10-162560 (2010).
41. Chen, J. *et al.* CCL18 from tumor-associated macrophages promotes breast cancer metastasis via PITPNM3. *Cancer Cell* **19**, 541–555, doi:10.1016/j.ccr.2011.02.006 (2011).
42. Chen, R. H. *et al.* Tumor Cell-Secreted ISG15 Promotes Tumor Cell Migration and Immune Suppression by Inducing the Macrophage M2-Like Phenotype. *Front Immunol* **11**, 594775, doi:10.3389/fimmu.2020.594775 (2020).
43. Huang, D. *et al.* Epstein-Barr Virus-Induced VEGF and GM-CSF Drive Nasopharyngeal Carcinoma Metastasis via Recruitment and Activation of Macrophages. *Cancer Res* **77**, 3591–3604, doi:10.1158/0008-5472.CAN-16-2706 (2017).

44. Su, S. *et al.* A positive feedback loop between mesenchymal-like cancer cells and macrophages is essential to breast cancer metastasis. *Cancer Cell* **25**, 605–620, doi:10.1016/j.ccr.2014.03.021 (2014).
45. Lane, D. *et al.* CCL18 from ascites promotes ovarian cancer cell migration through proline-rich tyrosine kinase 2 signaling. *Mol Cancer* **15**, 58, doi:10.1186/s12943-016-0542-2 (2016).
46. Vanheule, V., Metzemaekers, M., Janssens, R., Struyf, S. & Proost, P. How post-translational modifications influence the biological activity of chemokines. *Cytokine* **109**, 29–51, doi:10.1016/j.cyto.2018.02.026 (2018).
47. Greer, E. L. & Shi, Y. Histone methylation: a dynamic mark in health, disease and inheritance. *Nat Rev Genet* **13**, 343–357, doi:10.1038/nrg3173 (2012).

Figures

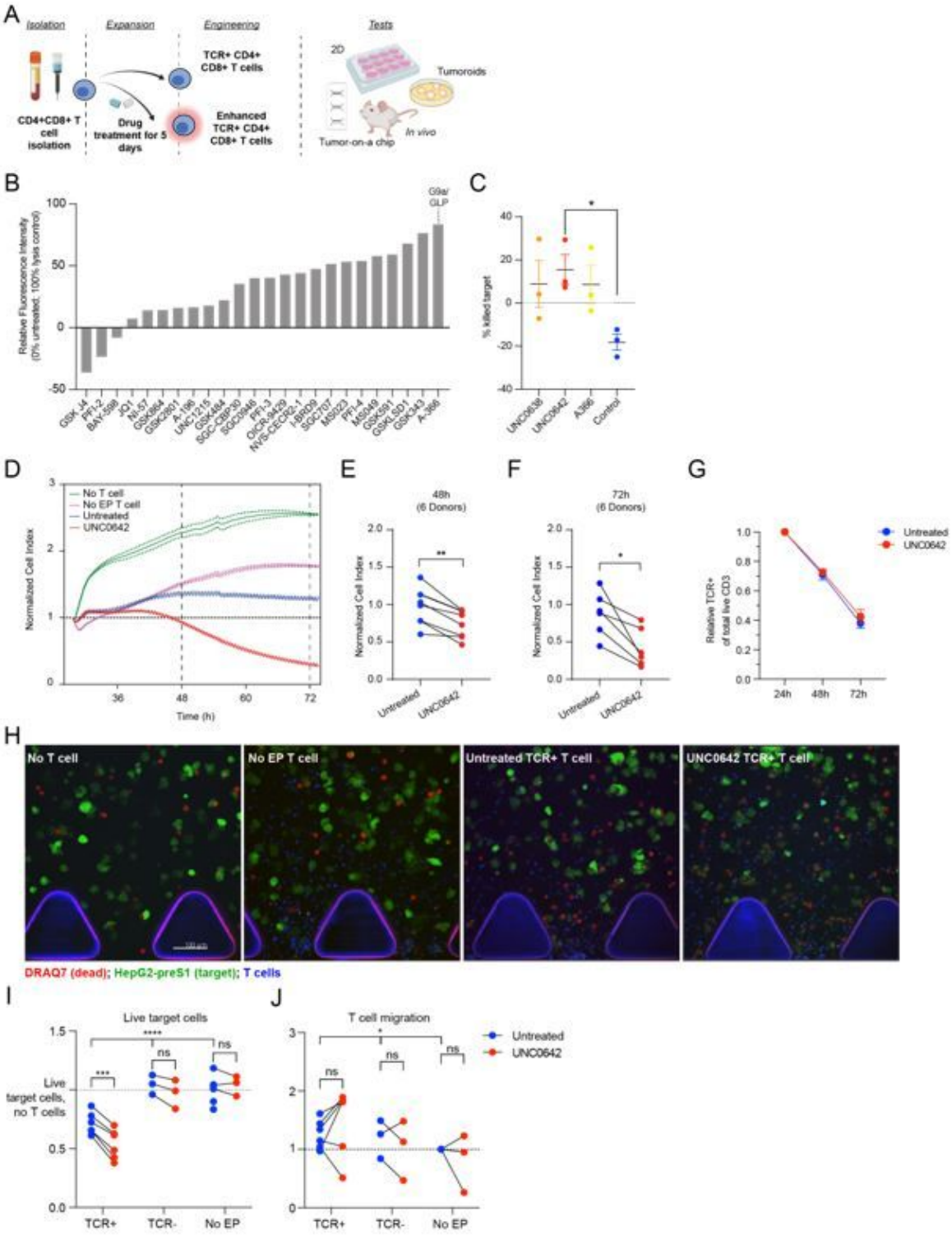

Figure 1

G9a/GLP inhibitors improve the cytotoxicity of TCR-engineered T cells. (A) Workflow for enhanced TCR T cell therapy formation and validation. (B) Relative cytotoxicity of T cells towards HepG2-preS1 target cells, after 5 days of treatment with a drug panel targeting epigenetic factors. Data at 48h after co-culture of T cells and target cells are shown. (C) TCR-engineered T cell cytotoxicity towards their target cell line after drug treatment in a 3D migration assay. UNC0642-treated T cells resulted in a significant increase in

target cell death compared to untreated T cells. (D) Representative image of 2D cell killing assay, tracked using xCelligence, with normalized cell index at (E) 48-hour and (F) 72-hour time point. (G) TCR expression levels in untreated and UNC0642-treated TCR^+ T cells after electroporation. (H) Representative image showing live (green) and dead (red) cells in 3D target cell killing assay, with quantification of (I) target cells alive after addition of untreated or UNC0642-treated TCR^+ T cells, TCR^- electroporated T cells (TCR^-) and naïve T cells (no EP), normalised to no T cell controls and (J) number of invading T cells within the 3D matrix. *P < 0.05, **P < 0.01, ***P < 0.001, ****P < 0.0001, ns = not significant.

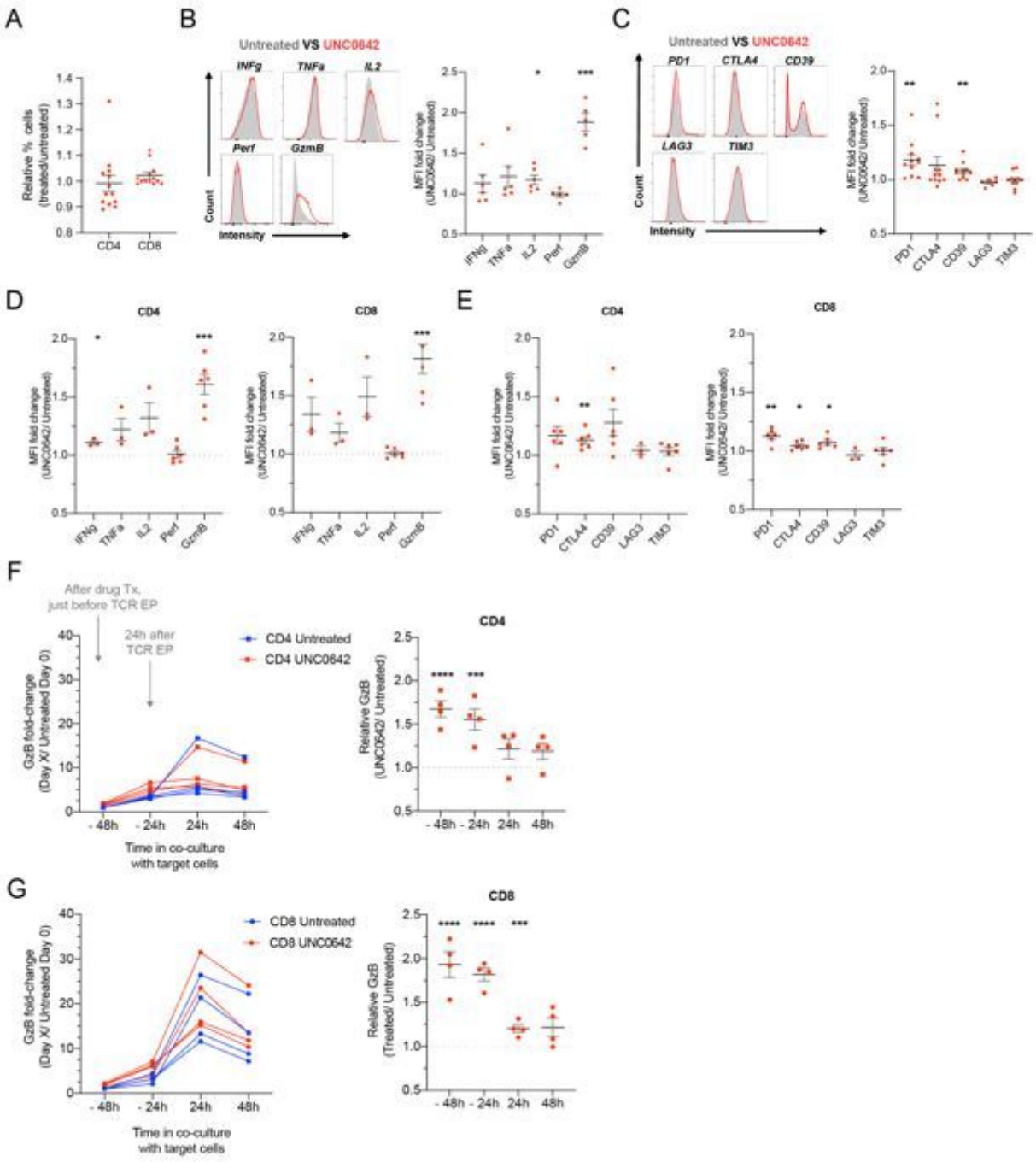

Figure 2

UNC0642 treatment increases the cytotoxicity and of TCR-engineered T cells. (A) Relative percentage of $CD4^+$ and $CD8^+$ T cells after UNC0642 treatment. Data are normalised to percentages in untreated paired samples. **(B)** Representative plot of flow cytometry data and quantification of effector and activation proteins after UNC0642 treatment. Data are normalised to percentages in untreated paired samples. **(C)** Representative plot of flow cytometry data and quantification of surface expression of proteins related to activation and exhaustion after UNC0642 treatment. Data are normalised to percentages in untreated paired samples. **(D)** MFI of effector and activation markers in $CD4^+$ and $CD8^+$ T cells after UNC0642 treatment. Data are normalised to percentages in untreated paired samples. **(E)** MFI of activation and exhaustion markers in $CD4^+$ and $CD8^+$ T cells after UNC0642 treatment. Data are normalised to percentages in untreated paired samples. **(F)** Granzyme B expression in untreated and UNC0642-treated TCR^+ $CD4^+$ T cells over time in co-culture with HepG2-preS1. Left panel: Data are normalised to untreated sample before TCR transfection at -48 h. Right panel: Data are normalised to untreated sample at each timepoint. **(G)** Granzyme B expression in untreated and UNC0642-treated TCR^+ $CD8^+$ T cells over time in co-culture with HepG2-preS1. *P < 0.05, **P < 0.01, ***P < 0.001, ****P < 0.0001.

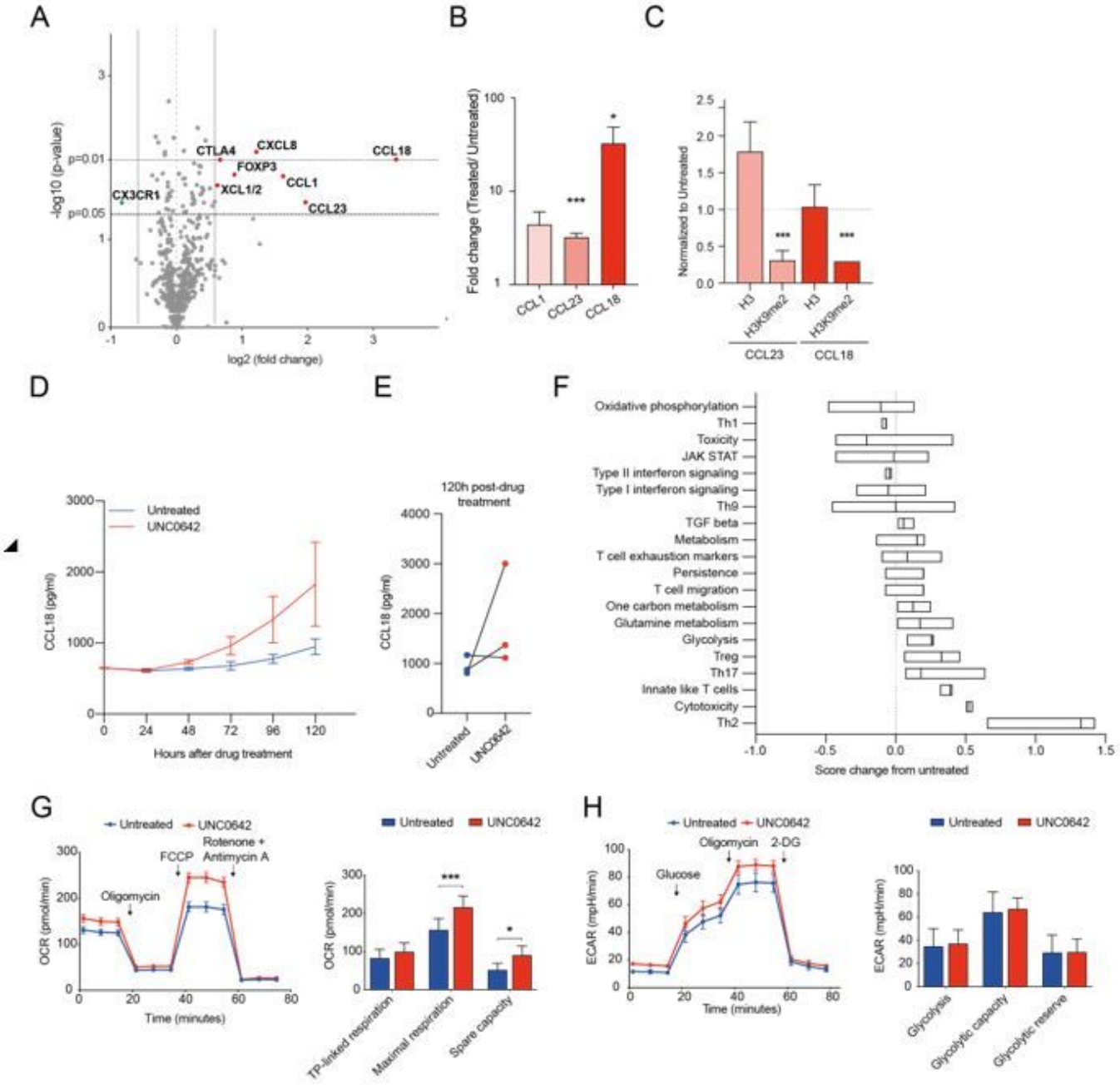

Figure 3

Gene expression changes after UNC0642 treatment assayed using Nanostring CAR-T characterisation panel. (A) Volcano plot of changes in gene expression assayed with Nanostring CAR-T characterisation panel for T cells after drug treatment (n=3 donors). Genes with a significant ($p < 0.05$) increase of greater than 1.5 fold are in red, and less than 1.5 fold in green. **(B)** qPCR validation of changes in gene expression after drug treatment. Data are represented as fold-change from untreated. Data are from 5 different donor T cells. **(C)** ChIP-qPCR validation of changes in H3K9me2 at *CCL28* and *CCL18* after drug treatment. Data are represented as fold-change from untreated. **(D)** Secreted CCL18 concentration after drug treatment assayed by ELISA. Data are represented as mean±SEM over time. **(E)** Secreted CCL18

concentration at 120h after drug treatment. Data for individual donors are shown. (**F**) Change in pathway scores after drug treatment. Pathway scores were defined using nSolver Advanced analysis software. Data are from 3 different donor T cells (n=3 donors). ()*P < 0.05, **P < 0.01, ***P < 0.001, ****P < 0.0001.

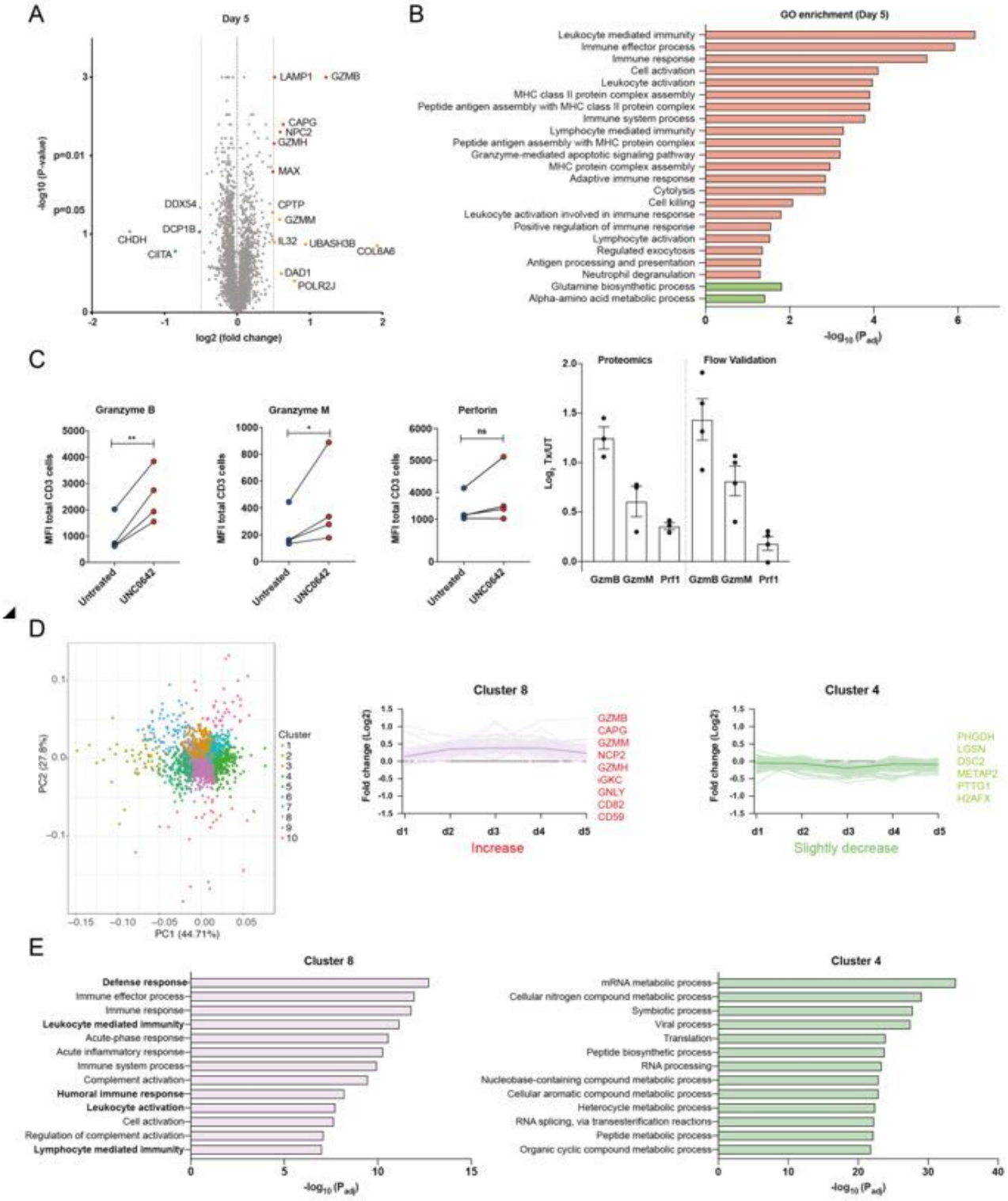

Figure 4

Changes in protein abundance in T cells after UNC0642 treatment assayed using TMT labelling (A) Changes in protein abundance of T cells after 5 days of UNC0642 treatment (n=3 donors). **(B)** Change in pathway scores after drug treatment of the differentially abundance proteins. Pathway scores were identified using Panther. Upregulated pathways are indicated in red and downregulated pathways are indicated in green. **(C)** Flow cytometry validation of changes in protein abundance in GZMB, GZMM and PRF1 after drug treatment. Left 3 panels: Data are non-normalised MFI reads. Right panel: Data are represented as fold-change from untreated paired samples. Data are from 3 different donor T cells. **(D)** Proteins grouped by changes in abundance over time using k-means clustering, represented on a PCA plot (left) and on a plot showing fold-change over time (right). **(E)** Change in pathway scores in the Cluster 8 (proteins increasing with the UNC0642 treatment) and 4 (proteins decreasing with UNC0642 treatment).

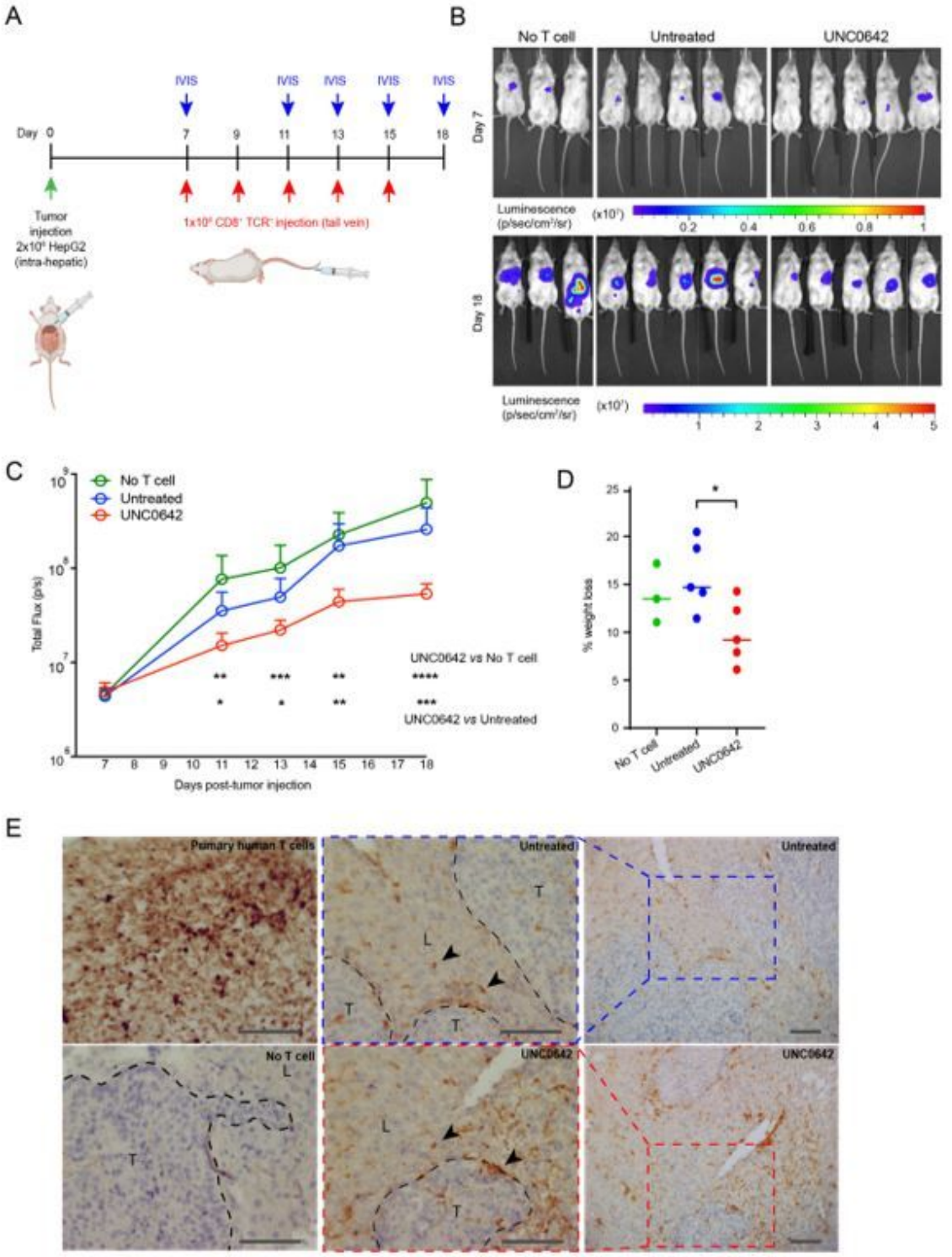

Figure 5

UNC0642 treatment improves the ani-tumor activity *in vivo*. (A) Overall design of *in vivo* experiment. 2M HepG2-2.2.15-luc cells were injected intra-hepatically at the start of the experiment. At day 7, mice were allocated in 3 groups and, subsequently, 1M of untreated or UNC0642-treated TCR+ T cells were injected intra-venously. The T cell injection was repeated every 2 days until day 15 post-tumor injection. Imaging was done using IVIS. **(B)** Representative images taken using the *in vivo* bioluminescence imaging system

at day 7 and at day 18 post-tumor injection. **(C)** Amount of tumor cells in the liver were tracked using luminescence and shown as total photon flux (p/s) over time. **(D)** Percentage loss of body weight. **(E)** Immunohistochemical images of liver sections stained for CD3 to identify T cells, with normal liver (L) and tumor (T) areas indicated. Primary human T cells serve as positive staining control and no T cell sample as negative staining control. Scale bar represents 50um. Arrowheads point to T cells. *P < 0.05, **P < 0.01, ***P < 0.001, ****P < 0.0001.

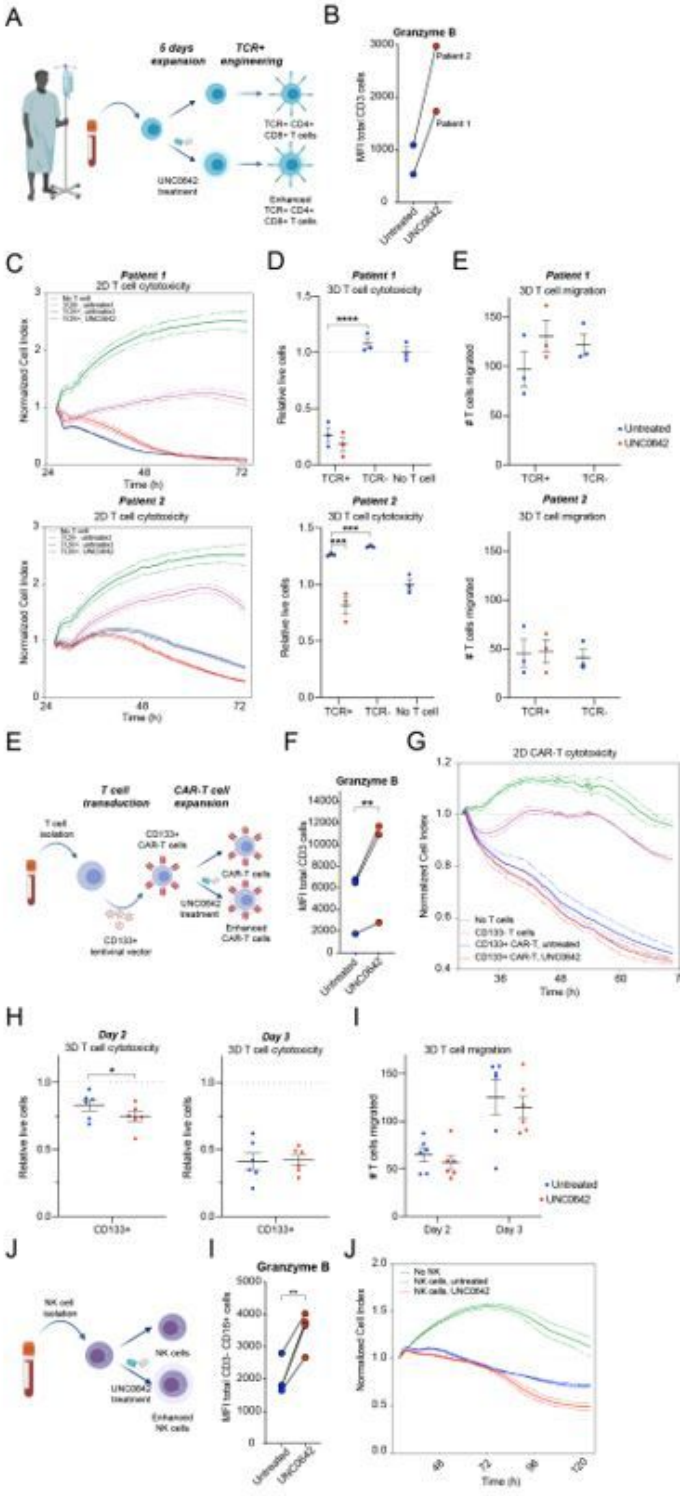

Figure 6

UNC0642 treatment increases the cytotoxicity of patients T cells, NK cells and CAR-T cells. (A) Workflow for enhanced patient T cell therapy formation and validation. **(B)** Granzyme B expression levels in patient T cells after UNC0642 treatment. **(C)** 2D target cell killing assay for Patient 1 (top panel) and Patient 2 (bottom panel). Data are normalized to cell index at time of T cell addition, and are represented as mean with standard error of the mean over time. **(D)** 3D target cell killing assay for Patient 1 and Patient 2. Data are normalized to no T cell target cell numbers. **(E)** T cell migration in 3D target cell killing assay for Patient 1 and Patient 2. **(E)** Workflow for $CD133^+$ CAR-T production and UNC0642 treatment. **(F)** Granzyme B expression levels in CAR-T cells after UNC0642 treatment. **(G)** 2D target cell killing assay for $CD133^-$ T cells, untreated $CD133^+$ CAR-T cells and UNC0642-treated $CD133^+$ CAR-T cells. **(H)** 3D target cell killing assay for untreated and treated $CD133^+$ CAR-T cells at day 2 and day 3. Data are normalized to no T cell target cell numbers. **(I)** T cell migration in 3D target cell killing assay for untreated and treated $CD133^+$ CAR-T cells at day 2 and day 3. **(J)** Workflow for NK isolation and UNC0642 treatment. **(F)** Granzyme B expression levels in NK cells after UNC0642 treatment. **(H)** 2D target cell killing assay for untreated and UNC0642-treated NK cells. *P < 0.05, **P < 0.01, ***P < 0.001, ****P < 0.0001.

Supplementary Files

This is a list of supplementary files associated with this preprint. Click to download.

- Supplementaryfiguresandmethods.docx